One-pot synthesis of Au-M@SiO_2 (M = Rh, Pd, Ir, Pt) core-shell nanoparticles as highly efficient catalysts for the reduction of 4-nitrophenol

Junfang Hao
Northwest University
Bin Liu
Northwest University
Shinya Maenosono
Japan Advanced Institute of Science and Technology
Jianhui Yang (jianhui@nwu.edu.cn)
Northwest University

Article

Keywords:

Posted Date: March 10th, 2022

DOI: https://doi.org/10.21203/rs.3.rs-1433157/v1

Abstract

The conversion of p-nitrophenol (4-NP) to p-aminophenol (4-AP) is of great significance for pharmaceutical and material manufacturing. In this work, Au-M@SiO_2 (M = Rh, Pd, Ir, Pt) nanoparticles (NPs) with core-shell structures, which are expected to be excellent catalysts for the transformation of 4-NP to 4-AP, were synthesized by a facile one-pot one-step method. The structure and composition of the NPs were characterized through transmission electron microscopy (TEM), X-ray powder diffraction (XRD) and X-ray photoelectron spectroscopy (XPS). Au-M@SiO_2 (M = Rh, Pd, Ir, Pt) core-shell NPs showed excellent catalytic activity in the reduction of 4-NP, which is superior to most catalysts reported in the previous literature. The enhanced catalytic activity of Au-M@SiO_2 core-shell NPs is presumably related to the bimetallic synergistic effect. This study provides a simple strategy to synthesize core-shell bimetallic NPs for catalytic applications.

Introduction

P-nitrophenol (4-NP) is a common organic pollutant, while its reduction product (p-aminophenol, 4-AP) has a wide range of applications in pharmaceuticals, dyestuffs, and high polymer material fields[1–3]. Therefore, the reduction reaction of 4-NP to 4-AP is of vital practical importance. However, this reaction is very slow without catalyst in the presence of $NaBH_4$[4]. In recent years, an increasing number of metal catalysts have been used for the reduction of 4-NP. Many investigations have focused on monometallic catalysts, such as Au, Ag, Pd, Cu, Ni and Co[5–10]. Compared to them, bimetallic catalysts exhibit better catalytic performance, such as Au-Pd alloy nanocrystals, silica (SiO_2)-coated Ag/Au nanoparticles (NPs) and MOF-supported Au@Ag core-shell NPs[11–13]. These can be ascribed to their unique morphology and optimized electronic structure by synergy or alloy effects[14–19]. Au catalysts are widely employed in many fields, for example, CO oxidation, coupling reactions, oxidation of ethanol and degradation of 4-NP, because they are most active and selective under mild or even low-temperature conditions at the nanoscale[20–23]. Moreover, platinum-group metals (PGMs, such as Rh, Pd, Ir and Pt) have excellent chemical activity and thus exhibit advantageous performance[24–27]. According to previous reports, bimetallic Au-PGMs nanomaterials have attracted extensive interest for many catalytic applications, such as cyclization reactions, electrocatalysis and CO oxidation[28–31]. For example, Lv's group reported ultrasmall Au@Pt core-shell nanostructures, which presented an enhanced performance for the hydrogen evolution reaction[32]. Mu's group synthesized Au/Pd heterojunction@mesoporous SiO_2 yolk-shell nanomaterials that exhibited high stability and plasmon-enhanced catalytic activity[33]. These results demonstrate that the combination of Au and PGMs is an effective way to enhance their catalytic performance. However, few reports have studied bimetallic Au-PGMs catalysts for the degradation of 4-NP. In addition, only bimetallic NPs tend to aggregate and leach during the reaction progress, resulting in decreased catalytic activity and stability[34,35]. Therefore, it would be a promising strategy to coat the surface of bimetallic Au-PGMs NPs with a SiO_2 shell to overcome these problems.

In this study, we used a one-pot one-step method to synthesize Au-M@SiO_2 (M = Rh, Pd, Ir, Pt) core-shell NPs. The stability of the catalyst was increased, and the agglomeration of NPs was prevented in the presence of the SiO_2 shell. The morphology and structure of the Au-M@SiO_2 core-shell NPs were determined by TEM, XRD and XPS. The catalytic performance of the Au-M@SiO_2 (M = Rh, Pd, Ir, Pt) core-shell NPs was investigated in the model reaction of the reduction of 4-NP. This work provides a simplified way to prepare SiO_2-coated bimetallic NP catalysts.

Results And Discussion

Here, Au-Rh@SiO_2 core-shell NPs are used as an example to illustrate the one-pot synthesis of silica-coated bimetallic Au-M (M = Rh, Pd, Ir and Pt) NPs. The morphology, structure and size of the samples were characterized by TEM. As shown in Fig. 1(a) and 1(b), the as-prepared sample possesses core-shell structure and good monodispersity. The elemental mapping analysis of the sample in Fig. 1(d-f) demonstrates that Rh is distributed uniformly in the side of Au, and Au-Rh NPs were coated by silica shell, which further affirms the formation of core-shell structure. It is concluded that Au-Rh@SiO_2 NPs with core-shell structures were synthesized successfully by this one-pot method. Au-Rh@SiO_2 NPs have a core-shell structure. To further clarify the crystalline structure between Au and Rh, Au-Rh NPs synthesized without TEOS were characterized by TEM and high-resolution TEM. As shown in Fig. S1 in the ESM (Electronic Supplementary Material), Au-Rh NPs with core-satellite structure are similar to some Rh “planets” around an Au core. The formation of this unique structure is mainly because of the immiscibility and lattice mismatch of Au and Rh[36]. There are some heterojunction structures at the boundary between Au and Rh, which could contribute to their electron interaction and further improve their catalytic performance.

The crystal structure of Au-Rh@SiO_2 core-shell NPs was obtained by XRD. As shown in Fig. 2(a), the main peaks at 38.6°, 45.0°, 65.2°, 78.1°, and 82.8° can be ascribed to the (111), (200), (220), (311), and (222) planes of Au (JCPDS: 04-0784)[37]. These peaks are in accordance with the peak positions of Au@SiO_2 in Fig. S2, indicating the formation of a nonalloyed structure. However, there are no characteristic peaks of Rh. This might be attributed to the fact that the particle size of Rh is too small to be obtained. The elemental composition and states of Au-Rh@SiO_2 core-shell NPs were further analyzed and characterized by XPS, as shown in Fig. 2(b). The main peaks of the Rh 3d spectrum can be deconvoluted into four peaks. The two peaks at 304.6 eV and 308.2 eV can be related to Rh $3d_{5/2}$ and Rh $3d_{3/2}$ of Rh (0), and those with binding energies of 306.5 eV and 312.2 eV can be related to Rh $3d_{5/2}$ and Rh $3d_{3/2}$ of Rh (III)[38,39]. Compared with the standard values, the peaks of Rh species shift to higher binding energies[40]. Moreover, through peak area integral calculation, the ratio of Rh (0) and Rh (III) was found to be 1.45. The peak of Au 4f is too weak to clearly observe in the survey-level XPS spectrum (Fig. S3), which is mainly because the Au-Rh “core-satellite” structure is coated by a silica shell[41]. This further confirmed the formation of a heterojunction structure rather than alloy, which is in agreement with the XRD result. The sample of Au-Rh NPs (Fig. S1) synthesized without TEOS was also characterized by XPS. As shown in Fig. S4, Au 4f core-level and Rh 3d core-level signals are present due to the absence of a silica shell. The

molar ratio of Au and Rh is 1.0 by the calculation of XPS peak areas, which is consistent with the molar ratio of their precursors. In addition, the two peaks of Au (0) shift to the lower binding energy, which is mainly due to the electron interaction between Au and Rh[32]. The electronegativity of Au is higher than that of Rh, which results in an increased electron density of Au and a reduction of electron binding energy. Comparing the XPS spectra of Au-Rh@SiO_2 core-shell and Au-Rh NPs, the ratio of Rh (0) and Rh (III) decreased from 1.45 to 0.75. This further revealed that the existence of silica shell could improve their stability.

The formation mechanism of Au-Rh@SiO_2 core-shell NPs was investigated by acquiring TEM images of the samples taken at different reaction times. Here, Au-Rh@SiO_2 core-shell NPs were synthesized by a one-pot one-step method developed by our research group and Zhao's group[42,43]. $HAuCl_4$ and $RhCl_3$ were reduced by formaldehyde to result in the formation of Au-Rh core-satellite NPs after the reacted solution was heated at 80°C for 5 min. At the same time, a thin layer of silica formed on the surface by base-catalyzed hydrolysis and polymerization of TEOS, as shown in Fig. 3(a). In Fig. 3(b), most of the Au-Rh NPs coated with a thin silica layer silica are on the outer edge of the silica spheres. The structures of the Au-Rh@SiO_2 core-shell NPs initially formed after 20 min of reaction, as shown in Fig. 3(c). However, Au-Rh NPs are not at the center of the silica spheres. At higher concentrations of CTAB, the lamellar micelles formed could induce anisotropic growth of SiO_2 shells on the surface and Au-Rh NPs[44]. As the consumption of CTAB, the spherical micelles adopted may result in the isotropic growth of SiO_2 shells. As shown in Fig. 3(d), Au-Rh@SiO_2 core-shell NPs finally formed at 60 min. The forming process mechanism of Au-Rh@SiO_2 core-shell NPs is illustrated in Fig. 3(e).

We also investigated the effect of different precursor ratios (1:2 and 2:1) of Au and Rh on the resulting NPs. The samples were defined as Au_1-Rh_2@SiO_2 and Au_2-Rh_1@SiO_2 core-shell NPs, which were synthesized with $HAuCl_4$ to $RhCl_3$ molar ratios of 1:2 and 2:1, respectively. As demonstrated in Fig. 4, the two samples are with core-shell structures, the core is Au-Rh bimetallic NPs, and the shell with similar thickness is silica. When we carefully checked the structure of Au-Rh bimetallic NPs, it could be clearly seen that Au-Rh bimetallic NPs with core-satellite structure and isolated Ru NPs were encapsulated in the center of silica for the Au_1-Rh_2@SiO_2 core-shell NPs in Fig. 4(a). For Au_2-Rh_1@SiO_2 core-shell NPs in Fig. 4(b), Au is not coated well with Rh particles and Au-Rh core-satellite structure is not formed in the center of the silica shell. Similarly, we also examined the molar ratio of Au and Rh in Au_1-Rh_2 and Au_2-Rh_1 bimetallic NPs without silica shells synthesized in the absence of TEOS by XPS. As shown in Fig. S5 and S6, the molar ratios of Au to Rh of Au_1-Rh_2 and Au_2-Rh_1 bimetallic NPs are 0.56 and 1.68 according to the calculation of the corresponding XPS peak areas, respectively.

We also employed this method to synthesize silica-coated bimetallic NPs consisting of Au and other platinum group metals (Pd, Ir, Pt). Figure 5(a, b, c) shows the TEM image, HAADF-STEM image and elemental mapping of Au-Pd@SiO_2, Au-Ir@SiO_2 and Au-Pt@SiO_2 core-shell NPs, respectively. Combined with the results of TEM and XRD characterizations of Au-Pd, Au-Ir and Au-Pt bimetallic NPs shown in Fig.

S7 and S8, Au-Pd@SiO_2, Au-Ir@SiO_2 and Au-Pt@SiO_2 core-shell NPs can be successfully synthesized using this one-pot one-step method simply by changing the corresponding metallic precursor.

To explore the catalytic reduction performance of 4-NP to 4-AP, UV–vis spectra in the presence of $NaBH_4$ during different reaction times were monitored. The UV–vis absorption peaks of 4-NP and 4-AP are located at 400 nm and 300 nm in Fig. S9, respectively. The UV–vis spectra of Au-Rh@SiO_2 core-shell NPs as a catalyst in Fig. 6(a) show that the reduction reaction of 4-NP finished within 5 min, indicating its good catalytic performance. The catalytic capability of Rh@SiO_2 (Fig. S10a), Au@SiO_2, and the mixture was further measured. Distinctly, in Fig. 6(b-d), in the presence of Rh@SiO_2, Au@SiO_2 and the mixture as a catalyst, this reaction finished within 8 min, 60 min and 13 min, respectively. The broad peak at approximately 500–550 nm comes from the surface resonance plasmon resonance of Au NPs (Fig. S11). This phenomenon exhibits that Au-Rh@SiO_2 core-shell NPs feature superior catalytic performance over their corresponding single component catalysts.

Table 1
Comparison of catalytic performance of bimetallic nanocatalysts for the reduction of 4-NP

Catalyst	Mass	Kinetic constant	References
MOF-supported Au@Ag core-shell NPs	—	0.298 min^{-1}	12
Au@Pd core-shell nanocubes	1 mL of 4.2×10^{10} particle/mL	2.05 ± 0.12 min^{-1}	46
Ni–Pt NPs	1 mL of 0.1 mg/mL	0.116 min^{-1}	47
Pd/Au(3:1)@g-C_3N_4-N	—	0.5310 min^{-1}	48
Au/Pd core/shell NPs	75 µL of 2.0 mM	0.32 min^{-1}	1
Cu/Ag alloy NPs	2 mg	0.237 min^{-1}	49
Au-Rh@SiO_2 core-shell structure	**1 mL of 0.019 mg/mL**	**0.826 min^{-1}**	**This work**

In addition, the investigation on kinetics of the catalysts were further analyzed. If the ratio of C_t/C_0 (4-NP concentration at t minutes and 0 min) is proportional to time, this reduction reaction could be seen as first order kinetic, and the slope of the fitting line is a first order kinetic constant[45]. The corresponding results are shown in Fig. 7. The first-order kinetic constants of Au-Rh@SiO_2 core-shell NPs, Rh@SiO_2, Au@SiO_2 and the mixture of Rh@SiO_2 and Au@SiO_2 NPs as catalysts are 0.826 min^{-1}, 0.276 min^{-1}, 0.037 min^{-1} and 0.228 min^{-1}, respectively. Clearly, Au-Rh@SiO_2 core-shell NPs have the maximum kinetic constant, also suggesting that this material exhibits the best catalytic performance. In addition, it can be observed from Table 1 that this catalyst is also superior to other bimetallic nanocatalysts reported in the previous literature[1,12,48–49], revealing its excellent catalytic activity.

According to the results of TEM and XPS characterization of the Au-Rh@SiO_2 core-shell NPs, Au-Rh bimetallic NPs exhibit core-satellite structures. There are some heterojunction structures at the boundary between Au and Rh, which result in their electron interaction and could improve their catalytic performance. To verify our hypothesis, the catalytic performance of Au-Rh@SiO_2 core-shell NPs with different molar ratios of Au and Rh in Fig. S12 and S13 show UV–vis spectra at different reaction times in the presence of Au_1-Rh_2@SiO_2 core-shell NPs and Au_2-Rh_1@SiO_2 core-shell NPs. Figure 8 plots ln (C_t/C_0) vs. time in the presence of Au-Rh@SiO_2 core-shell NPs with different molar ratios of Au and Rh. Compared with the kinetic constant of Au-Rh@SiO_2 core-shell NPs, Au_2-Rh_1@SiO_2 core-shell NPs exhibited the lowest catalytic performance due to the low content of Rh. However, for the sample of Au_1-Rh_2@SiO_2 core-shell NPs, its catalytic performance was still lower than that of Au-Rh@SiO_2 core-shell NPs. As observed in Fig. 3(a), a thicker layer of Rh NPs was formed and prevented the synergistic effect of Au and Rh. In conclusion, the Au-Rh@SiO_2 core-shell NPs as highly efficient catalysts for the reduction of 4-NP could be attributed to the synergistic effect coming from their unique core-shell structure and electronic interaction of Au and Rh.

The synergistic effect was also confirmed by other silica-coated Au-based PGMs bimetallic NPs. Fig. S14-17 show the catalytic performance of Au-M@SiO_2 (M = Pd, Ir, Pt) core-shell NPs for the reduction of 4-NP. They exhibit highly efficient catalytic activity with first-order kinetic constants of 0.359 min^{-1}, 0.100 min^{-1} and 0.135 min^{-1}, respectively. As shown in Fig. 9, we summarized the Au-M@SiO_2 (M = Rh, Pd, Ir, Pt) core-shell NPs as catalysts for the reduction of 4-NP. Au-Rh@SiO_2 core-shell NPs exhibit the highest catalytic activity for the reduction of 4-NP in the excess of $NaBH_4$, which is due to the higher adsorption energy of 4-NP on Rh surfaces and more efficient interfacial electron transfer between Au and Rh.

Conclusions

In summary, Au-M@SiO_2 (M = Rh, Pd, Ir, Pt) NPs with core-shell structures were successfully synthesized by a facile one-pot one-step method. The morphology, crystal structure, elemental composition and formation mechanism of these core-shell NPs were investigated. Au-M@SiO_2 (M = Rh, Pd, Ir, Pt) core-shell NPs showed excellent catalytic activity in the reduction of 4-NP, which is superior to most catalysts reported in the previous literature. The enhanced catalytic activity of Au-M@SiO_2 core-shell NPs is presumably related to the bimetallic synergistic effect. This study provides a simple strategy to synthesize core-shell bimetallic NPs for catalytic applications.

Methods

Materials. Chloroauric acid tetrahydrate ($HAuCl_4 \cdot 4H_2O$, ≥47.0%, Beijing Huawei Ruike Chemical Co., Ltd), palladium chloride acid (H_2PdCl_4, > 97.0%, Shanghai Macklin Biochemical Co., Ltd), chloroplatinic acid hexahydrate ($H_2PtCl_6 \cdot 6H_2O$, ≥ 37.0%, Shanghai Institute of Fine Chemical Materials), rhodium chloride trihydrate ($RhCl_3 \cdot 3H_2O$, ≥ 39.0%, Xi'an Kaili Chemical Co., Ltd), cetyltrimethylammonium bromide (CTAB,

$C_{19}H_{42}BrN$, 97.0%, Shanghai Macklin Biochemical Co., Ltd), iridium trichloride ($IrCl_3$, ≥ 42.5%, Shanghai Bide Pharmaceutical Technology Co., Ltd), sodium hydroxide (NaOH, ≥ 96.0%, Tianjin Tianli Chemical Reagent Co., Ltd), formaldehyde solution (HCHO, 37.0%-40.0%, Tianjin Fuyu Chemical Reagent Co., Ltd), 4-NP ($C_6H_5NO_3$, 99%, Damas-beta Reagent Co., Ltd), sodium borohydride ($NaBH_4$, Tianjin Cameo Chemical Reagent Co., Ltd.) and tetraethyl orthosilicate (TEOS, Tianjin Cameo Chemical Reagent Co., Ltd.) were directly used without further purification. Anhydrous alcohol and deionized water were used in all experiments.

Synthesis. Au@SiO_2 core-shell NPs were synthesized by a facile one-pot one-step method using formaldehyde as a reducing agent[42,43]. Similarly, M@SiO_2 (M = Rh, Pd, Ir and Pt) core-shell NPs were prepared by changing the corresponding metal precursors.

The above method is still suitable for the synthesis of bimetallic Au-M@SiO_2 (M = Rh, Pd, Ir and Pt) core-shell NPs. Taking Au-Rh@SiO_2 core-shell NPs as an example, in a typical synthesis, 38 mL of deionized water, 6 mL of ethanol, 0.07 g of CTAB, 1 mL of HCHO, 1 mL of NaOH (0.5 mol/L), 1 mL of 8.14 mmol/L $HAuCl_4$, 1 mL of 8.14 mmol/L $RhCl_3$ and 0.10 mL of TEOS were mixed in a 100 mL of beaker under ultrasonication. The beaker was left in an oil bath at 80°C for 60 min under stirring. After cooling to room temperature naturally, the product was centrifuged at 11,000 rpm for 20 min and washed two times with water to remove the surfactant and unreacted chemicals. Finally, the precipitate was dissolved in 3 mL of water for further characterization.

Au-Rh@SiO_2 core-shell NPs with different Au/Rh molar ratios were obtained under the same reaction conditions by changing the molar ratio of $HAuCl_4$ to $RhCl_3$ to 1:2 and 2:1, respectively.

The other Au-M@SiO_2 (M = Pd, Ir and Pt) core-shell NPs were prepared by replacing $RhCl_3$ with H_2PdCl_4, $RhCl_3$ and H_2PtCl_6, respectively.

The procedure of preparing Au-M (M = Rh, Pd, Ir and Pt) bimetallic NPs is similar to the typical synthesis of Au-Rh@SiO_2 core-shell NPs in the absence of TEOS.

Characterization. Transmission electron microscopy (TEM) images were obtained from Talos F200X (FEI, 200 kV) equipped with a high-angle annular dark field (HAADF) detector and an energy dispersive X-ray (EDX) spectrometer. The TEM samples were prepared by dropping nanoparticle dispersions onto 200-mesh copper grids covered with carbon membranes. X-ray diffraction (XRD) measurements were carried out on a Bruker D8 Advance diffractometer with Cu Kα radiation (λ = 1.54059 Å). X-ray photoelectron spectrophotometer (XPS) spectra were taken by using a PHI5000 Versa Probe III spectrometer with an excitation source of Al Kα. The samples for XRD and XPS were prepared by dropping nanoparticle dispersion onto silicon wafers and dried naturally at room temperature. All spectra were recalibrated with respect to the C 1s core level peak at 284.8 eV of carbon contamination. UV–vis absorption spectra were obtained on an ultraviolet–visible spectrophotometer (SP-75).

Catalytic reduction of 4-nitrophenol. 1 mL of freshly prepared $NaBH_4$ (0.06 mol/L) was mixed with 1 mL of 4-NP (1.7×10^{-4} mol/L) in a quartz cuvette with 1 cm path length. The detailed illustration takes Au-Rh@SiO_2 NPs as an example. 1 mL of Au-M@SiO_2 core-shell NP aqueous dispersion was quickly added to the above solution. The catalytic reaction progress of the conversion of 4-NP to 4-AP was observed via UV–vis spectroscopy between 250 and 600 nm at ambient temperature.

Declarations

Acknowledgements

This work was supported by the Education Commission of Shaanxi Province (No. 2022JM-086). J. Yang thanks the Cyrus Tang Foundation (China) for Tang Scholar.

Author contributions

J. H: Conceptualization, Methodology, Investigation, and Writing-original draft. B. L: Conceptualization, Methodology, and Writing-Review&Editing. S. M: Investigation, Validation, and Writing-Review&Editing. J.Y: Conceptualization, Supervision, Visualization and Writing-Review&Editing. All authors reviewed the manuscript.

Competing interests

The authors declare no competing interests.

Additional information

Supplementary Information The online version contains supplementary material available.

Correspondence and requests for materials should be addressed to S. M. and J.Y.

References

1. Srisombat, L., Nonkumwong, J., Suwannarat, K., Kuntalue, B. & Ananta, S. Simple preparation Au/Pd core/shell nanoparticles for 4-nitrophenol reduction. Colloids Surf. A Physicochem. Eng. Asp. **512**, 17–25 (2017).
2. Serrà, A., Artal, R., Pozo, M., Garcia-Amorós, J. & Gómez, E. Simple environmentally-friendly reduction of 4-nitrophenol. Catalysts **10**, 458–469 (2020).
3. Wang, Y. N. *et al.* One-pot green synthesis of bimetallic hollow palladium-platinum nanotubes for enhanced catalytic reduction of p-nitrophenol. J. Colloid Interface Sci. **539**, 161–167 (2019).
4. Zhao, P. X., Feng, X. W., Huang, D. S., Yang, G. Y. & Astruc, D. Basic concepts and recent advances in nitrophenol reduction by gold- and other transition metal nanoparticles. Coord. Chem. Rev. **287**, 114–136 (2015).

5. Lin, F. H. & Doong, R. A. Highly efficient reduction of 4-nitrophenol by heterostructured gold-magnetite nanocatalysts. Appl. Catal. A Gen. **486**, 32–41 (2014).
6. Dubey, S. P. *et al.* Synthesis of graphene-carbon sphere hybrid aerogel with silver nanoparticles and its catalytic and adsorption applications. *Chem. Eng. J.* **244**, 160–167 (2014).
7. Liu, T. *et al.* Pd nanoparticle-decorated 3D-printed hierarchically porous TiO_2 scaffolds for the efficient reduction of a highly concentrated 4-nitrophenol solution. *ACS Appl. Mater. Interfaces* **12**, 28100–28109 (2020).
8. Jia, W. L. *et al.* Nitrogen-doped porous carbon-encapsulated copper composite for efficient reduction of 4-nitrophenol. J. Colloid Interface Sci. **594**, 254–264 (2021).
9. Jiang, Z. F., Xie, J. M., Jiang, D. L., Wei, X. J. & Chen, M. Modifiers-assisted formation of nickel nanoparticles and their catalytic application to p-nitrophenol reduction. CrystEngComm **15**, 560–569 (2013).
10. Zhang,Y. X. *et al.* Active cobalt induced high catalytic performances of cobalt ferrite nanobrushes for the reduction of p-nitrophenol. J. Colloid Interface Sci. **535**, 499–504 (2019).
11. Zhang, J. W. *et al.* Surfactant-concentration-dependent shape evolution of Au-Pd alloy nanocrystals from rhombic dodecahedron to trisoctahedron and hexoctahedron. Small **9**, 538–544 (2013).
12. Jiang, H. L., Akita, T., Ishida, T., Haruta, M. & Xu, Q. Synergistic catalysis of Au@Ag core-shell nanoparticles stabilized on metal-organic framework. J. Am. Chem. Soc. **133**, 1304–1306 (2011).
13. Chen, Y., Wang, Q. H. & Wang, T. M. Fabrication of thermally stable and active bimetallic Au-Ag nanoparticles stabilized on inner wall of mesoporous silica shell. Dalton Trans. **42**, 13940–13947 (2013).
14. Ma, T., Liang, F., Chen, R. S., Liu, S. M. & Zhang, H. J. Synthesis of Au-Pd bimetallic nanoflowers for catalytic reduction of 4-nitrophenol. Nanomaterials **7**, 239–247 (2017).
15. Zhang, H. J. & Toshima, N. Synthesis of Au/Pt bimetallic nanoparticles with a Pt-rich shell and their high catalytic activities for aerobic glucose oxidation. J. Colloid Interface Sci. **394**, 166–176 (2013).
16. Patnaik, S., Sahoo, D. P. & Parida, K. M. Bimetallic co-effect of Au-Pd alloyed nanoparticles on mesoporous silica modified g-C_3N_4 for single and simultaneous photocatalytic oxidation of phenol and reduction of hexavalent chromium. J. Colloid Interface Sci. **560**, 519–535 (2020).
17. Pozun, Z. D. *et al.* A systematic investigation of p-nitrophenol reduction by bimetallic dendrimer encapsulated nanoparticles. J. Phys. Chem. C **117**, 7598–7604 (2013).
18. Suwannarat, K., Thongthai, K., Ananta, S. & Srisombat, L. Synthesis of hollow trimetallic Ag/Au/Pd nanoparticles for reduction of 4-nitrophenol. Colloids Surf. A Physicochem. Eng. Asp. **540**, 73–80 (2018).
19. Endo, T., Yoshimura, T. & Esumi, K. Synthesis and catalytic activity of gold-silver binary nanoparticles stabilized by PAMAM dendrimer. J. Colloid Interface Sci. **286**, 602–609 (2005).
20. Shanmugaraj, K., Bustamante, T. M., Torres, C. C. & Campos, C. H. Gold nanoparticles supported on mesostructured oxides for the enhanced catalytic reduction of 4-nitrophenol in water. Catal. Today

388–389, 383–393 (2020).

21. Seo, Y. S. *et al.* Catalytic reduction of 4-nitrophenol with gold nanoparticles synthesized by caffeic acid. Nanoscale Res. Lett. **12**, 7–17 (2017).
22. Li, F., Zhou, H. P., Fan, J. J. & Xiang, Q. J. Amine-functionalized graphitic carbon nitride decorated with small-sized Au nanoparticles for photocatalytic CO_2 reduction. J. Colloid Interface Sci. **570**, 11–19 (2020).
23. Sarkodie, B. *et al.* Highly efficient Au/Fe_2O_3 for CO oxidation: the vital role of spongy Fe_2O_3 toward high catalytic activity and stability. J. Colloid Interface Sci. **608**, 2181–2191 (2022).
24. Yang, Y. *et al.* NIR-II driven plasmon-enhanced catalysis for a timely supply of oxygen to overcome hypoxia-induced radiotherapy tolerance. Angew. Chem. Int. Ed. **58**, 15069–15075 (2019).
25. Oh, H. S., Nong, H. N., Reier, T. Gliech, M. & Strasser, P. Oxide-supported Ir nanodendrites with high activity and durability for the oxygen evolution reaction in acid PEM water electrolyzers. Chem. Sci. **6**, 3321–3328 (2015).
26. Wang, J. *et al.* One-step and rapid synthesis of "clean" and monodisperse dendritic Pt nanoparticles and their high performance toward methanol oxidation and p-nitrophenol reduction. Nanoscale **4**, 1549–1552 (2012).
27. Guo, Y. *et al.* Pore structure dependent activity and durability of mesoporous rhodium nanoparticles towards the methanol oxidation reaction. Chem. Commun. **56**, 4448–4451 (2020).
28. Du, C. *et al.* Epitaxial growth of zigzag PtAu alloy surface on Au nano-pentagrams with enhanced Pt utilization and electrocatalytic performance toward ethanol oxidation reaction. Electrochim. Acta **238**, 263–268 (2017).
29. Lv, F. *et al.* A convenient detection system consisting of efficient Au@PtRu nanozymes and alcohol oxidase for highly sensitive alcohol biosensing. Nanoscale Adv. **2**, 1583–1589 (2020).
30. Liang, Z. X. *et al.* Direct 12-electron oxidation of ethanol on a ternary Au(core)-PtIr(Shell) electrocatalyst. J. Am. Chem. Soc. **141**, 9629–9636 (2019).
31. Wagh, S. B., Hsu, Y. C. & Liu, R. S. Two distinct cyclizations of 2-propenyl-1-ethynyl benzenes with aryldiazo esters using Au and Rh/Au catalysts respectively. ACS Catal. **6**, 7160–7166 (2016).
32. Germano, L .D., Marangoni, V. S., Mogili, N. V. V., Seixas, L. & Maroneze, C. M. Ultrasmall (< 2 nm) Au@Pt nanostructures: tuning the surface electronic states for electrocatalysis. ACS Appl. Mater. Interfaces **11**, 5661–5667 (2019).
33. Mu, Y. J., Zhang, H. Y., Zheng, W. T. & Cui, X. Q. Highly stable Au/Pd@mesoporous SiO_2 yolk-shell hetero-nanostructures for plasmon-enhanced visible light driven catalytic reactions. New J. Chem. **41**, 786–792 (2017).
34. Bahadur, N. M. *et al.* Rapid one-step synthesis, characterization and functionalization of silica coated gold nanoparticles. Colloids Surf. A Physicochem. Eng. Asp. **392**, 137–144 (2011).
35. Lee, I., Joo, J. B., Yin, Y. D. & Zaera, F. A yolk@shell nanoarchitecture for Au/TiO_2 catalysts. Angew. Chem. Int. Ed. **50**, 10208–10211 (2011).

36. Piccolo, L. *et al.* Understanding and controlling the structure and segregation behaviour of AuRh nanocatalysts. Sci. Rep. **6**, 35226 (2016).
37. Huang, J. S., Han, X. Y., Wang, D. W., Liu, D. & You, T. Y. Facile synthesis of dendritic gold nanostructures with hyperbranched architectures and their electrocatalytic activity toward ethanol oxidation. ACS Appl. Mater. Interfaces **5**, 9148–9154 (2013).
38. Tabet-Aoul, A., Wang, H. X., Wang, Y. L. & Mohamedi, M. 3D porous sphere-like aggregates of bimetallic PtRh nanoparticles grown onto carbon nanotubes: efficient and durable catalyst for the ethanol oxidation reaction. J. Electrochem. Soc. **164**, F685-F693 (2017).
39. Meng, X. Y. *et al.* Distance synergy of MoS_2-confined rhodium atoms for highly efficient hydrogen evolution. Angew. Chem. Int. Ed. **59**, 10502–10507 (2020).
40. Bai, J., Xing, S. H., Zeng, J. H., Jiang, J. X. & Chen, Y. Hydrothermal synthesis and catalytic application of ultrathin rhodium nanosheet nanoassemblies. ACS Appl. Mater. Interfaces **8**, 33635–33641 (2016).
41. Liu, Y. S., Zhang, W., Li, X. L., Le, X. D. & Ma, J. T. Catalysis of the hydro-dechlorination of 4-chlorophenol and the reduction of 4-nitrophenol by Pd/Fe_3O_4@SiO_2@m-SiO_2. New J. Chem. **39**, 6474–6481 (2015).
42. Chen, J. C., Zhang, R. Y., Han, L., Tu, B. & Zhao, D. Y. One-pot synthesis of thermally stable gold@mesoporous silica core-shell nanospheres with catalytic activity. Nano Res. **6**, 871–879 (2013).
43. Zhang, S., Xu, X. C., Zhang, G. Y., Liu, B. & Yang, J. H. One-pot one-step synthesis of Au@SiO_2 core–shell nanoparticles and their shell-thickness-dependent fluorescent properties. RSC Adv. **9**, 17674–17678 (2019).
44. Vega, M. S., Martinez, A. G. & Cucinotta, F. Facile strategy for the synthesis of Gold@silica hybrid nanoparticles with controlled porosity and Janus morphology. Nanomaterials **9**, 348–366 (2019).
45. Hu, H. W., Xin, J. H., Hu, H. & Wang, X. W. Structural and mechanistic understanding of an active and durable graphene carbocatalyst for reduction of 4-nitrophenol at room temperature. Nano Res. **8**, 3992–4006 (2015).
46. Cui, Y. et al. Atomic-level insights into strain effect on p-nitrophenol reduction via Au@Pd core-shell nanocubes as an ideal platform. J. Catal. **381**, 427–433 (2020).
47. Ghosh, S. K., Mandal, M., Kundu, S., Nath, S. & Pal, T. Bimetallic Pt-Ni nanoparticles can catalyze reduction of aromatic nitro compounds by sodium borohydride in aqueous solution. Appl. Catal. A Gen. **268**, 61–66 (2004).
48. Fang, W. *et al.* Synthesis of Pd/Au bimetallic nanoparticle-loaded ultrathin graphitic carbon nitride nanosheets for highly efficientcatalytic reduction of p-nitrophenol. J. Colloid Interface Sci. **490**, 834–843 (2017).
49. Wu, W. *et al.* A one-pot route to the synthesis of alloyed Cu/Ag bimetallic nanoparticles with different mass ratios for catalytic reduction of 4-nitrophenol. J. Mater. Chem. A **3**, 3450–3455 (2015).

Figures

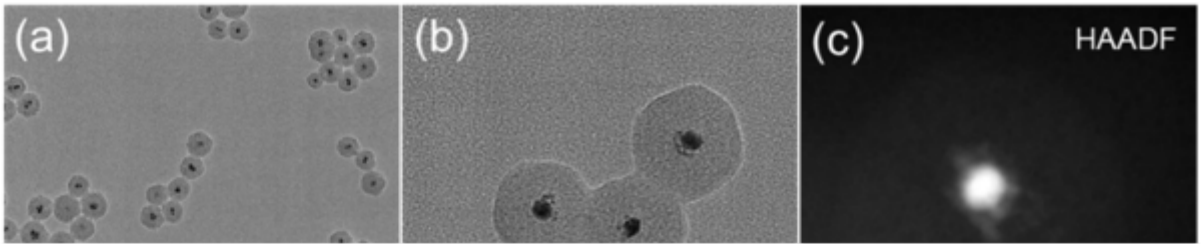

Figure 1

(a, b) TEM, (c) HAADF-STEM and (d-f) elemental mapping images of Au-Rh@SiO_2 core-shell NPs.

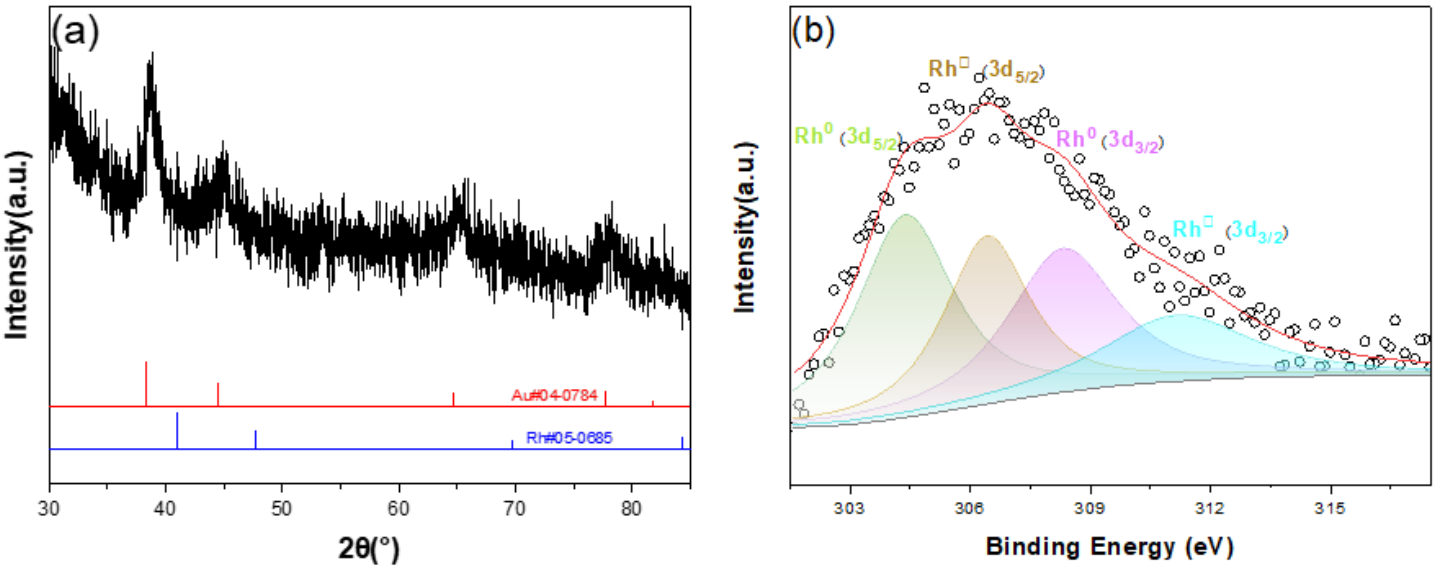

Figure 2

(a) XRD pattern and (b) Rh 3d spectrum of Au-Rh@SiO_2 core-shell NPs.

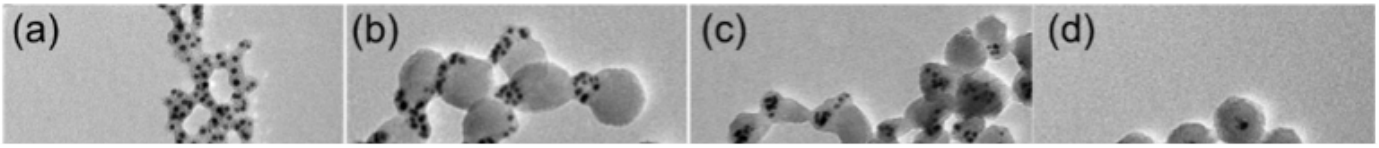

Figure 3

TEM images of the Au-Rh@SiO_2 core-shell NPs at different reaction time: (a) 5 min, (b) 10 min, (c) 20 min and (d) 60 min. The forming process mechanism illustration of Au-Rh@SiO_2 core-shell NPs (e).

Figure 4

TEM images, HAADF-STEM image, and elemental mapping of (a) Au_1-Rh_2@SiO_2 and (b) Au_2-Rh_1@SiO_2 core-shell NPs, respectively.

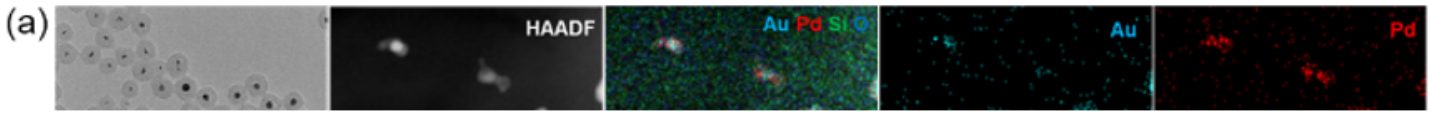

Figure 5

TEM image, HAADF-STEM image and elemental mapping of (a) Au-Pd@SiO_2, (b) Au-Ir@SiO_2 and (c) Au-Pt@SiO_2 core-shell NPs, respectively.

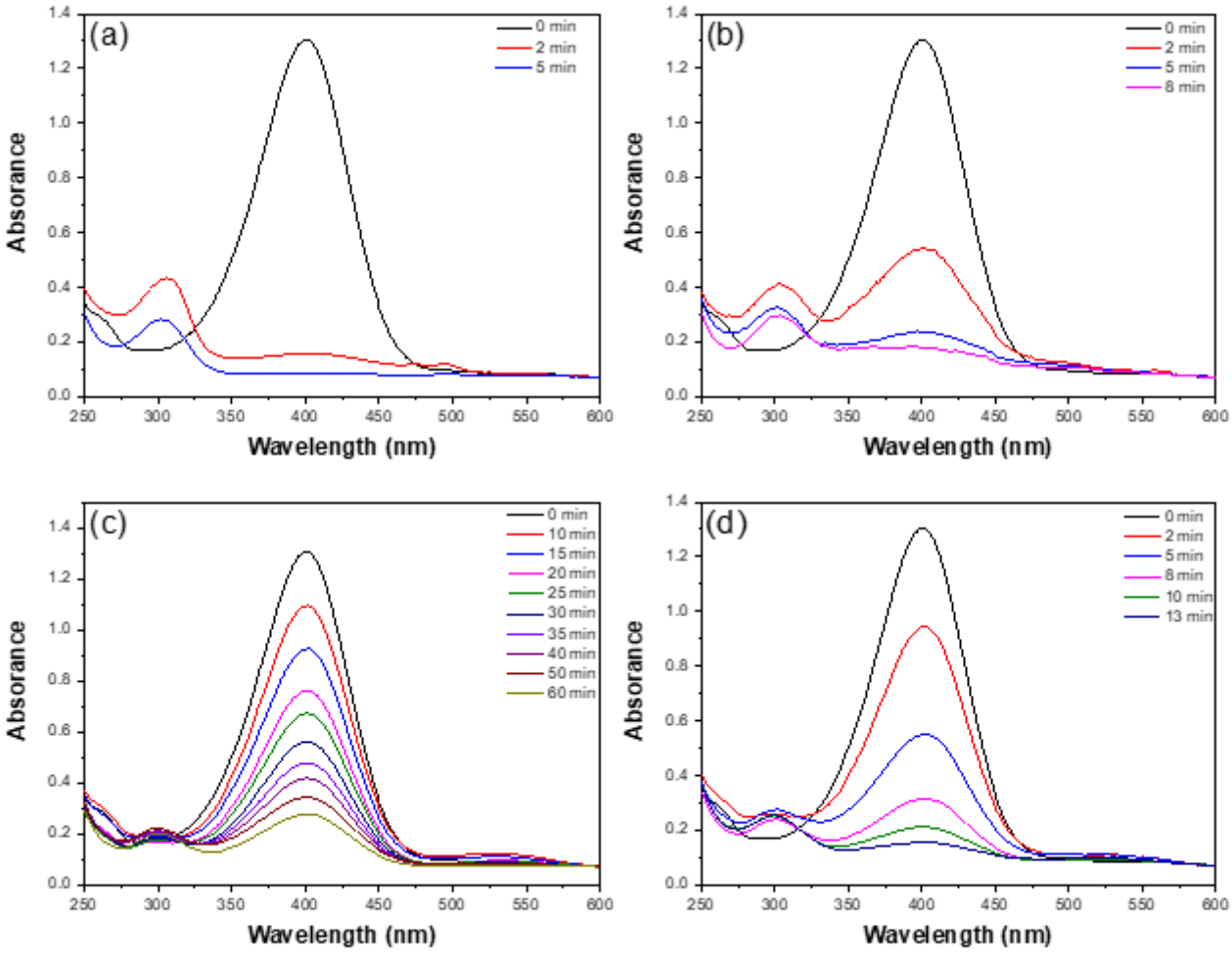

Figure 6

UV-vis spectra at different reaction times in the presence of Au-Rh@SiO_2 core-shell NPs (a), Rh@SiO_2 core-shell NPs (b), Au@SiO_2 core-shell NPs (c) and the mixture of Rh@SiO_2 and Au@SiO_2 core-shell NPs (d), respectively.

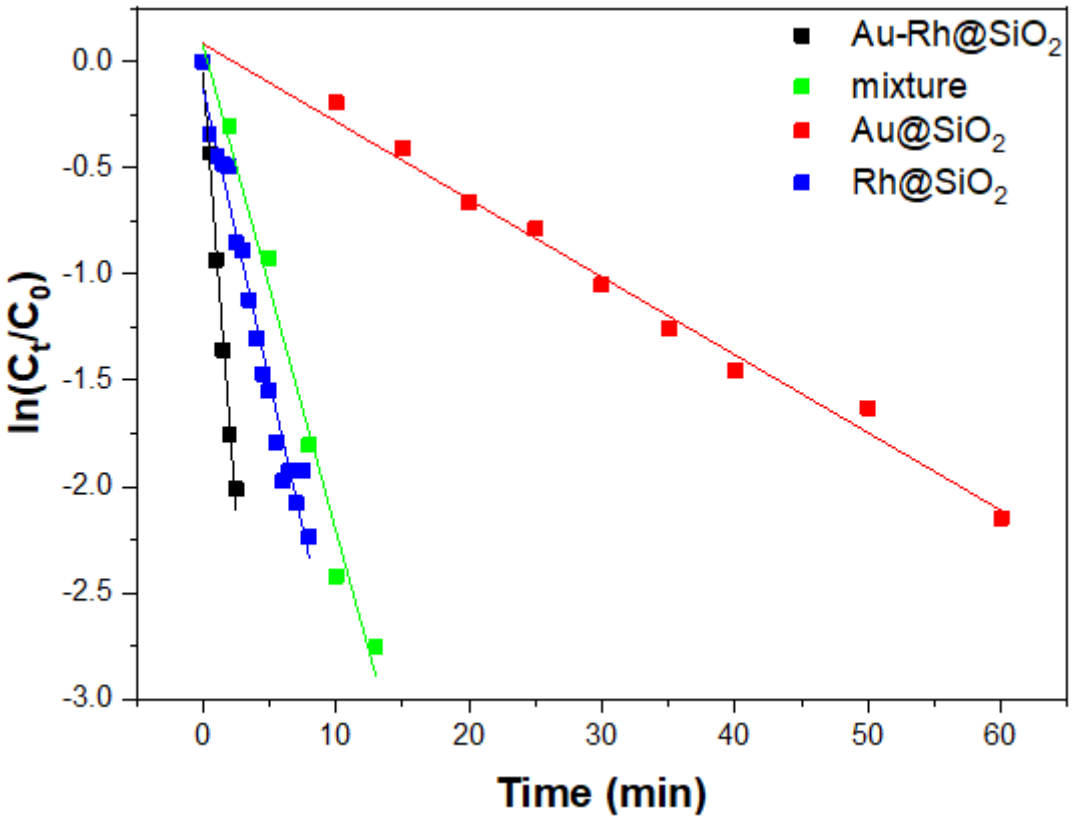

Figure 7

Plots of ln (C_t/C_0) vs. time in the presence of Au-Rh@SiO_2 core-shell NPs, Rh@SiO_2 core-shell NPs, Au@SiO_2 core-shell NPs and the mixture of Rh@SiO_2 and Au@SiO_2 core-shell NPs as catalysts.

Figure 8

Plots of ln (C_t/C_0) vs. time in the presence of Au_1-Rh_2@SiO_2 core-shell NPs, Au-Rh@SiO_2 core-shell NPs, Au_2-Rh_1@SiO_2 core-shell NPs.

Figure 9

The catalytic performance of Au-M@SiO_2 (M = Rh, Pd, Ir, Pt) core-shell NPs for reduction of 4-NP.

Supplementary Files

This is a list of supplementary files associated with this preprint. Click to download.

- Electronicsupplementarymaterial.pdf